

Relativistic versus Newtonian orbit model: the Relativistic Motion Integrator (RMI) software. Illustration with the LISA mission.

Sophie Pireaux[§] Bertrand Chauvineau[¶] and Aurelien Hees^{||}
*Observatoire Royal de Belgique (ORB),
Observatoire de la Côte d'Azur (OCA)*

25th June, 2009

Abstract. The Relativistic Motion Integrator (RMI) consists in integrating numerically the EXACT relativistic equations of motion, for a given metric (corresponding to a gravitational field at first post-Newtonian order or higher), instead of Newtonian equations plus relativistic corrections.

The aim of the present paper is to validate the method, and to illustrate how RMI can be used for space missions to produce relativistic ephemerides of test-bodies (or satellites). Indeed, nowadays, relativistic effects have to be taken into account, and comparing a RMI model with a classical keplerian one helps to quantify such effects.

LISA is a relevant example to use RMI. This mission is an interferometer formed by three spacecraft which aims at the detection of gravitational waves. A precise orbit model for the LISA spacecraft is needed not only for the sake of satellite ephemerides but also to compute the photon flight time in laser links between spacecraft, required in LISA data pre-processing in order to reach the gravitational wave detection level.

Relativistic effects in LISA orbit model needed to be considered and quantified. Using RMI, we show that the numerical classical model for LISA orbits in the gravitational field of a non-rotating spherical Sun without planets can be wrong, with respect to the numerical relativistic version of the same model, by as much as about ten kilometers in radial distance during a year and up to about 60 kilometers in along track distance after a year... with consequences on estimated photon flight times.

We validated RMI numerical results (using a metric following the International Astronomical Union -IAU- 2000 resolutions) with an analytical development (up to first order in eccentricity and up to first order in GM/c^2 , where G is Newton's constant, M , the solar mass and c the speed of light in vacuum).

Finally, the RMI relativistic numerical approach is soon more efficient than the analytical development. Moreover, RMI extends to other cases (planetocentric, instead of barycentric) and can be applied to other space missions.

Keywords: relativity, ephemeris, orbit model, IAU conventions.

[§] Department 1

Observatoire Royal de Belgique, 3 avenue Cirulaire, 1180 BRUSSELS, BELGIUM.

Tel: ++32(0)2 373 67 53 and Fax: ++32(0)2 374 98 22. E-mail: sophie.pireaux@oma.be

Previously working in UMR 6162, ARTEMIS, OCA.

[¶] UMR 6162, ARTEMIS,

Observatoire de la Côte d'Azur (OCA), avenue de Copernic, 06130 GRASSE, FRANCE.

^{||} Department 1

Observatoire Royal de Belgique, 3 avenue Cirulaire, 1180 BRUSSELS, BELGIUM.



1. Introduction

Due to considerable increase of the accuracy level in modern space missions in the recent years, or expected in close-future missions, relativistic gravitational effects must be considered when computing spacecraft ephemerides.

Indeed, the Schwarzschild radius ($2GM/c^2$) of the Earth is of the order of one centimeter; while that of the Sun is of the order three kilometers. The first corresponds to the order of magnitude of the precision in current space geodesy; while the second, to the precision requested in some future space mission such as in LISA (2015). The relativistic Lense-Thirring effect has already been partially detected with LA-GEOS Earth orbiting satellites (Ciufolini & Pavlis 2004). Numerical integrations in the post-Newtonian approximation versus Newtonian ones have shown the relevance of relativistic effects in the orbit of the future GAIA mission (2011) (Klioner 2005), since the GAIA spacecraft must be controlled with an accuracy of 0.6mm/s. Owing to the above motivations, the present work is dedicated to a numerical relativistic model for a generic space mission.

The method RMI (Relativistic Motion Integrator), a fully consistent general relativistic approach (Pireaux et al. 2005), (Pireaux et al. 2006) consists in integrating numerically the EXACT relativistic equations of motion for a given metric. The advantages of the method are the following. All relevant relativistic effects are taken into account if a gravitational metric adapted to the precision of measurements is chosen. The approach is relativistically consistent, and safer than adding relativistic corrections by hand to a computation first developed in a Newtonian framework. The RMI approach *natively* contains all the gravitational classical and relativistic effects at the corresponding order of the metric, including all the couplings between these effects at the corresponding order with respect to the metric chosen. This is a serious advantage over a Newtonian-plus-relativistic-corrections approach such as is implemented in commonly used orbit determination softwares. These perturbation approaches become more and more questionable as the requested precision increases, requiring a larger number of relativistic effects to be taken into account. RMI could help to point out deficiencies in common softwares.

The standard approach to integrate the relativistic differential equations of motion are the Einstein-Infeld-Hoffmann (EIH) equations of motion (see (Brumberg 1992), (Brumberg 2004), (Brumberg 2007), (Damour et al. 1991), (Damour et al. 1992), (Damour et al. 1993), (Damour et al. 1994), (Moyer 2000) and references therein). EIH equa-

tions are an analytical first order post-Newtonian (1PN) development of the exact relativistic equations of motion. The advantage of the RMI method over the standard integration of EIH equations is that RMI straightaway numerically integrates the equations of motion for a chosen metric provided at a given PN order (whether 1PN or higher). Hence, if, according to new IAU (or else) resolutions, a more appropriate/precise metric than the present Barycentric Coordinate Reference System (BCRS) metric for the motion in the Solar System or Geocentric Coordinate Reference System (GCRS) metric for planetocentric motion (with the Earth as central body) is recommended, RMI can straight away use that new metric... without the need to recalculate and implement new analytical developments. Only the metric module in the RMI software changes. Indeed, separate modules in the RMI numerical method also allow easy adaptations and updates for a given mission (number of plane containing satellites, number of satellites per plane, initial conditions -positions and velocities-), central body parameters (mass multipole development of the gravitational potential, spin), planetary ephemerides, IAU recommendations (metric, space-time transformations)... while keeping the main body of the software unchanged.

When wishing to illustrate how the RMI method can be used in space missions, LISA is a good candidate. However, the aim of the present paper is not to provide a thorough model of the LISA detector. Although some results obtained with RMI for LISA's orbit model are relevant for a LISA simulator.

The LISA (Laser Interferometer Space Antenna) mission (LISA 2000) is a space detector of gravitational waves in the $[\sim 10^{-4}, \sim 10^{-1}]$ Hz frequency band. Gravitational waves crossing the LISA quasi equilateral triangular constellation are detected through the induced change in the station inter-distances. The latter also depend on time, mainly due to the gravitational field of the Sun (Chauvineau et al. 2005) around which LISA rotates, 20 degrees behind the Earth, and to that corresponding to planets; what we call “geometry effects”.

“Noise effects” in LISA are orders of magnitude larger than “gravitational wave source effects”. In order to reach the gravitational wave detection level, a Time Delay Interferometry (TDI) method (see (Dhurandhar et al. 2002), (Estabrook et al. 2000)) must be applied to get rid of (most of) the laser frequency noise and optical bench noise. The TDI method consists in combining numerically data fluxes at the stations (rather than combining the laser beams physically) with an appropriate delay. Hence, the so-called TDI observables are symmetrized combinations of the different laser links with appropriate delays (combination

of photon-flight time between two stations which correspond to station inter-distances) that cancel (almost all) the laser frequency noise and optical bench noise. The TDI method is the crucial pre-processing of LISA data, before even trying a given strategy to detect any gravitational wave signal.

Therefore, in order to validate the new TDI technique and since a laboratory replica of the complex LISA mission is not totally achievable, the performance of LISA TDI can only be studied with computer simulations of the different processes involved. Such is the aim of the LISACode software [(Petiteau et al. 2008)] developed by the LISAFrance group [(LISA-France 2009)], or of other simulators in the USA [(Vallisneri 2005), (Cornish et al. 2004)]. Among the processes to be implemented in a LISA simulator, the orbit model of the spacecraft, providing positions, velocities and interdistances of spacecraft needed for TDI, is the subject of the present paper.

Relativistic effects in LISA needed to be considered and quantified. In the framework of the LISA mission, in articles (Chauvineau et al. 2005) (see references therein for a generic approach) and (Pireaux 2007), the photon flight time problem, also sometimes referred to as time transfer, and proper time scales of LISA spacecraft are tackled using a consistent general *relativistic* approach. However, the orbit model used to compute the initial positions and velocities of LISA spacecraft at emission time needed in the time transfer simulation or in proper-versus-coordinate time transformations is *classical*.

And so is it still presently the case too in the TDI simulators named Synthetic LISA (Vallisneri 2005), LISA Simulator (Cornish et al. 2004) and LISACode (Petiteau et al. 2008).

In the preliminary optimal orbit design for LISA used by Hughes (Hughes 2005), LISA's orbit model is also purely classical (in presence of a spherical non-rotating Sun with planets). The author looks for the optimal set of orbital inclinations, eccentricities, semi-major axis, longitude of the ascending nodes, arguments of perigee and initial mean anomalies $(a_k, e_k, i_k, \Omega_k, \omega_k, M_{k0})$ of LISA spacecraft ($k = 1, 2, 3$) in order to minimize LISA's arm flexing according to certain optimization criteria.

In the present article, we use RMI (assuming no non-gravitational forces for LISA spacecraft motion) to quantify the errors implied when a classical orbit model is adopted for LISA instead of a general relativistic one for the same initial conditions (Barycentric Coordinate Reference System -BCRS- positions and velocities of spacecraft). We first investigate the case of a classical *circular* orbit of reference around a spherical non-rotating Sun without planets, which we call the *circular spherical symmetric case*. We then extend to *eccentric* orbits and name this case the *eccentric spherical symmetric case* (more specifically for

LISA, $e \simeq 0.0096$).

Our numerical estimate of relativistic versus Keplerian orbit model for LISA with $e = 0.0096$ shows that the difference between predicted barycentric relativistic and classical radial distance reaches up to about $8 - 9$ km during a one-year mission and that the along track difference in orbits is about $54 - 59$ km after one year (i.e. after one classical period), according to the spacecraft considered, in the eccentric spherical symmetric case.

The relativistic versus classical modelling of LISA's orbit has repercussions on the flexing of LISA interferometric arms, the so-called breathing of the LISA constellation around its nominal arm-length value $L = 5 \cdot 10^9$ m. We show that a relativistic orbit model is relevant when studying photon time transfer needed in the TDI method; more specifically because the zeroth order is but the spacecraft inter-distance divided by the speed of light.

Since LISA eccentricity is small and because TDI and classical orbit models for LISA used by the Mock LISA Data Challenge (MLDC) (Arnaud et al. 2007) task force have been developed using first-order in eccentricity approximations, we provide a relativistic analytical check: a development up to first order in eccentricity and up to first order in GM/c^2 , where G is Newton's constant, M , the solar mass and c the speed of light in vacuum) circular or eccentric spherical symmetric cases.

For the circular spherical symmetric case, the analytical development up to first order in e and GM/c^2 (equations (11) and (12)) leads to small residuals (about 1 cm in x-y-positions or along track distance and a few millimeters in radius) with respect to the RMI numerical relativistic model for LISA. However, in the eccentric spherical symmetric case, even for a small eccentricity such as LISA's ($e \simeq 0.0096$), the corresponding residuals are non negligible (reaching up to about 85 m in along track distance) due to the e^2 and higher terms neglected in the analytical development; whereas RMI implicitly contains all order in e . Hence, the analytical development is soon surpassed by the numerical relativistic approach of RMI. This remark is even more relevant to space missions with important eccentricities.

The RMI method was furthermore validated in reference (Hees & Pireaux (2009)) (for BepiColombo or MarsNext mission) using a full 1PN development.

The present paper is organized as follows. In Section 2, we recall the classical orbit model for LISA around a spherical symmetric Sun, which is to be our trial example for RMI along this paper.

In Section 3, we summarize the RMI relativistic numerical method and apply it to LISA with the appropriate initial conditions corresponding to the classical model. The numerical results obtained for LISA are then discussed.

In Section 4, we provide an analytical developpement (up to first order in eccentricity and in GM/c^2) to check RMI.

Finally, in Section 5, we conclude on the relevance of the RMI approach and on the main results obtained for LISA.

The annex A discusses the numerical accuracy of the RMI method for LISA.

We adopt Einstein's summation convention on repeated indices. Latin indices are for space coordinates, such as $l = 1, 2, 3$; while Greek indices are for space-time coordinates, such as $\alpha = 0, 1, 2, 3$ with $x^{\alpha=0,1,2,3} = (c \cdot t, x, y, z)$.

2. LISA classical orbit model in the spherical symmetric case

Presently, within simulators testing LISA TDI (in the framework of the LMDC (Arnaud et al. 2007)), the following simplifications relative to LISA orbits are assumed. Each spacecraft follows perfectly a free-falling test mass that is itself perfectly shielded from non-gravitational forces and feels no constraints (for simplicity, one test-mass per spacecraft is modeled). As the gravitational field is concerned, solely a spherical non-rotating Sun is considered. The orbit model is classical.

In present LISA simulators for TDI, departures from the above assumptions on orbits are presently considered as part of the noise budget in TDI: among residual laser frequency and optical bench noises, scattered-light noise, detector shot noise, laser-beam pointing instability, acceleration noise, inertial noise and others (as specified in Table 1 of reference (Petiteau et al. 2008)).

For such a classical orbit model for the three LISA spacecraft $k = 1, 2, 3$, in the BCRS, as in (Dhurandhar et al. 2005), the barycentric coordinates (x_k, y_k, z_k) , for arbitrary initial conditions, can be rewritten in terms of rotated Keplerian ellipses $(x_{ell\ k}, y_{ell\ k}, z_{ell\ k})$ with eccentricity $e \simeq 0.0096$ as

$$\begin{pmatrix} x_k \\ y_k \\ z_k \end{pmatrix} = \mathfrak{R}^{-1} \begin{pmatrix} x_{ell\ k} \\ y_{ell\ k} \\ z_{ell\ k} \end{pmatrix} \quad (1)$$

with

$$\begin{pmatrix} x_{ell\ k} \\ y_{ell\ k} \\ z_{ell\ k} \end{pmatrix} \equiv \begin{pmatrix} a (\cos \Psi_k - e) \\ a \sqrt{1 - e^2} \sin \Psi_k \\ 0 \end{pmatrix}$$

where a , e , i and ω are the common semi-major axis, eccentricity, inclination and argument of the periastron of the three spacecraft orbits, respectively; and

$$\mathcal{R}^{-1} \equiv (\varphi_1 \ \varphi_2 \ \varphi_3) ,$$

where the columns of the inverse rotation matrix are given by

$$\begin{aligned} \varphi_1 &\equiv \begin{pmatrix} +\cos \Omega_k \cos \omega - \sin \Omega_k \sin \omega \cos i \\ +\sin \Omega_k \cos \omega + \cos \Omega_k \sin \omega \cos i \\ +\sin \omega \sin i \end{pmatrix} , \\ \varphi_2 &\equiv \begin{pmatrix} -\cos \Omega_k \sin \omega - \sin \Omega_k \cos \omega \cos i \\ -\sin \Omega_k \sin \omega + \cos \Omega_k \cos \omega \cos i \\ +\cos \omega \sin i \end{pmatrix} , \\ \varphi_3 &\equiv \begin{pmatrix} +\sin \Omega_k \sin i \\ -\cos \Omega_k \sin i \\ +\cos i \end{pmatrix} . \end{aligned}$$

Indeed, we start from a slightly different hypothesis with respect to Hughes' (Hughes 2005). We take common (a, e, i) for the three spacecraft with optimal e , i in order to minimize LISA's arm flexing in agreement with reference (Nayak et al. 2006):

$$a = 1 \text{ A.U.},$$

$$e = \sqrt{1 + \frac{4}{\sqrt{3}} \frac{L}{2a} \cos \nu + \frac{4}{3} \left(\frac{L}{2a} \right)^2} - 1,$$

$$i = \arctg \left(\frac{\frac{L}{2a} \sin \nu}{\sqrt{3}/2 + \frac{L}{2a} \cos \nu} \right)$$

where $\nu = \frac{\pi}{3} + \frac{5}{8} \frac{L}{2a}$ is the optimal inclination of the LISA triangle on the ecliptic and $L = 5 \cdot 10^9$ m is the average interferometric arm-length. The longitude of the ascending node, Ω_k , is particular to a given spacecraft k and is given in terms of that of the first one with a phase shift ϑ_k :

$$\Omega_k = \Omega_1 - \vartheta_k \quad \text{with } \vartheta_k \equiv -2(k-1) \frac{\pi}{3}.$$

The time parametrization of the orbits is given by the equation of the eccentric anomaly Ψ_k of each spacecraft,

$$\Psi_k - e \sin \Psi_k = M_k , \tag{2}$$

with the mean anomaly

$$M_k = \frac{2\pi}{T} (t - t_0) + M_{k0}$$

in terms of the orbital period, T , and the mean anomaly of spacecraft k at initial time t_0 , that is $M_{k0} \equiv M_k(t = t_0)$.

Mean anomalies are related to that of the first spacecraft through the phase shift:

$$M_k = M_1 + \vartheta_k .$$

BCRS position and eccentric anomaly equations used in (Chauvineau et al. 2005) correspond to particular initial conditions ($t_0 = 0$, $\omega = 3\pi/2$, $\Omega_1 = 3\pi/2$, $M_{10} = 0$) without any planets (which means that both the initial time, t_0 , and the initial mean anomaly of the first spacecraft, M_{10} , are completely arbitrary in that case).

We also recall that the time when spacecraft k is at perihelion is given by

$$t_{kp} = t_0 - \frac{M_{k0}}{n}$$

with the mean motion $n \equiv 2\pi/T = \sqrt{GM/a^3}$ from Kepler's 3rd law.

3. Numerical *native* relativistic orbit model

3.1. EXACT RELATIVISTIC EQUATIONS OF MOTION

In General Relativity, the motion of a spacecraft is described by the relativistic equation of motion,

$$\frac{d^2 x^\alpha}{d\tau^2} = -\Gamma_{\beta\gamma}^\alpha \cdot \frac{dx^\beta}{d\tau} \cdot \frac{dx^\gamma}{d\tau} + K_\beta \left[g^{\alpha\beta} - \frac{dx^\alpha}{d\tau} \cdot \frac{dx^\beta}{d\tau} \right] \quad (3)$$

where K_β is a quadri-“force” encoding non-gravitational forces; τ , the proper time aboard the considered spacecraft; and $\Gamma_{\beta\gamma}^\alpha$, Christoffel symbols with respect to the metric. The relation between covariant and contravariant metric components being

$$g^{\alpha\beta} \cdot g_{\beta\gamma} = \delta_\gamma^\alpha . \quad (4)$$

The four equations in (3) are redundant because of the normalization of the quadrivelocity.

In the case of LISA, assuming only one shielded test-mass per satellite, each satellite follows a geodesic motion, that is $K_\beta = 0$. Combining equations in (3), we can remove the proper time variable to rewrite the set of relativistic equations as

$$\frac{d^2 x^l}{dt^2} = \left[-\Gamma_{\beta\gamma}^l + \frac{1}{c} \Gamma_{\beta\gamma}^0 \cdot \frac{dx^l}{dt} \right] \cdot \frac{dx^\beta}{dt} \cdot \frac{dx^\gamma}{dt} \quad (5)$$

3.2. RELATIVISTIC MOTION INTEGRATOR (RMI) METHOD APPLIED TO LISA

The Relativistic Motion Integrator (RMI) method (Pireaux et al. 2005), (Pireaux et al. 2006), consists in integrating numerically the *exact* relativistic equations of motion (3) for a given metric.

The numerical accuracy and stability of the RMI method for the LISA mission is validated in Annex A.

When using the RMI method for LISA, rotating around the Sun, the appropriate metric is the BCRS metric recommended by the IAU, International Astronomical Union, 2000 resolutions (see (Soffel et al. 2003) and references therein) and the corresponding isotropic coordinates. The BCRS IAU 2000 metric neglects only terms at order $1/c^5$ and above in g^{00} or g^{0l} ; and at order $1/c^4$ and above in g^{lm} . The IAU 2000 resolutions have been adopted in 2000 so to take into account the best precision of present and next future space experiments. That is experiments involving (or which can be translated in terms of) clocks, with accuracies better than a few parts in 10^{17} in fractional frequency and stabilities better than about $\sigma_y(\tau) = 1 \cdot 10^{-14} \tau^{-1/2}$ (Allan standard deviation), located at distances as close as 0.25 A.U. from the Sun (Soffel et al. 2003).

Note that most NASA and ESA space missions are modeled according to the EIH equations and corresponding relativistic algorithms described e.g. in (Moyer 2000). Unfortunately, reference (Moyer 2000) was published around October 2000 and thus does not take into account the latest IAU2000 resolutions, published later. (Moyer 2000) refers to IERS 1997 resolutions at the latest.

3.3. LISA INITIAL CONDITIONS

We shall use the subscript $*_{cl}$ for classical quantities and $*_{rel}$ for the relativistic ones.

In our problem of comparing relativistic and classical LISA ephemerides (E), we chose to take the same initial conditions (IC) in terms of coordinate positions and velocities of spacecraft $k = 1, 2, 3$ for both the relativistic and the classical orbits. Indeed, we could have chosen to speak in terms of same energy and momentum, but this does not reflect the way the actual space mission will be planned and this does not easily provide insight in terms of what is the error in predicted position and velocities. Hence, initial conditions of the relativistic model will be those BCRS $(x_k, y_k, z_k; dx_k/dt, dy_k/dt, dz_k/dt)$ obtained by setting $t = t_0$ in the classical equations (1) and (2).

Note that this choice is not restrictive since, if the classical and relativistic IC differ,

$$E_{rel}(IC_{rel}) - E_{cl}(IC_{cl}) = [E_{rel}(IC_{rel}) - E_{cl}(IC_{rel})] + [E_{cl}(IC_{rel}) - E_{cl}(IC_{cl})]$$

and the second r.h.s. term in the above equation, not discussed in this paper, is but a classical problem.

The eccentricity of the numerical ephemerides for the eccentric case is that corresponding to LISA spacecraft, $e \simeq 0.0096$. In our numerical simulation, we arbitrarily further chose $t_0 = 0$, $\omega = 3\pi/2$, $\Omega_1 = 3\pi/2$ and $M_{10} = 0$ in agreement with the initial conditions of paper (Chauvineau et al. 2005).

Let us point out that this analysis could have been applied to Hughes' initial conditions (Hughes 2005).

3.4. DISCUSSING NUMERICAL RESULTS FOR LISA IN THE SPHERICAL SYMMETRIC CASE

The spherical symmetric model for LISA corresponds to a classical orbit of reference around a spherical non-rotating Sun without planets. Owing to this symmetry, the value of the inclination i is irrelevant in order to compare relativistic versus classical ephemerides generated for LISA. Hence, we used the classical method without planets, described in Section 2, with i set to 0 and e set to either 0 (circular case) or 0.0096 (eccentric case), to produce a numerical classical ephemeris for LISA $(x_k, y_k, z_k, dx_k/dt, dy_k/dt, dz_k/dt)_t$. We then used the RMI method, described in the above Paragraphs 3.2 and 3.3 with identical initial conditions, to produce a corresponding relativistic numerical ephemeris. We then used those two ephemerides, recorded as a function of BCRS time, to plot (relativistic - classical) quantities as a function of BCRS time every day during 365 days ($\simeq T = 2\pi/n$) such as in Section 6.

3.4.1. Circular classical reference orbit case:

From Figures 1 and 2, we found that the difference between predicted barycentric relativistic and classical x-y-positions reaches up to a maximum of about 51 – 56 km during a one-year mission.

When speaking in terms of a difference in radial or along track distance between numerical relativistic and classical orbits, the above cited results translate into Figures 3 and 4, respectively. We computed that the maximum difference in radius is about 8.9 km while the along track difference in orbits after one classical period is about 56 km for this circular spherical symmetric case.

The spacecraft is ahead on the classical orbit with respect to the relativistic one.

We see from Figure 3 that, having adopted a circular classical orbit of

reference, the corresponding relativistic orbit is non-circular. The difference in velocity components along the x- or y-BCRS axis as a function of time obtained are given in Figures 5 and 6, respectively. The difference between predicted barycentric relativistic and classical x-y-velocities reaches up to a maximum of about $0.007 - 0.010$ m/s during a one-year mission. This agrees with the order of magnitude for the difference in position over one year.

3.4.2. *Eccentric ($e = 0.0096$) classical reference orbit case:*

From Figure 7, we see that the maximum difference in radius between numerical relativistic and classical orbits is about $8 - 9$ km, according to the spacecraft considered. From Figure 8, we see that the along track difference in orbits after one classical period reaches about -59 or -54 km, according to the spacecraft considered, for this eccentric spherical symmetric case.

3.4.3. *LISA's arm flexing and photon time transfer:*

Assuming $e = 0.0096$ and using the numeric relativistic ephemerides for LISA spacecraft obtained with the RMI method or that obtained with a classical method, we can compute the interferometric-arm length L_{jk} , that is the interdistance between spacecraft j and k . Over a year, LISA constellation shows some breathing or triangle flexing: the relative position of spacecraft varies as a function of time. It is interesting to see that, for the uninclined ($i = 0$) eccentric spherical symmetric model, the classical approach is wrong by as much as about 4 km over a one-year mission. However, the true mission has an inclination i such as to minimize the breathing (Nayak et al. 2006). Figure 15 illustrates LISA breathing in the inclined (with the appropriate i given in Section 2) eccentric spherical symmetric case. In that realistic model, the classical approach is wrong by as much as about 3 km over year of mission, as shown by the residuals (relativistic - classical) relative positions of spacecraft in Figure 16. This error translates into a missing $\sim 1 \cdot 10^{-5}$ s at zeroth order in $GM/(a c^2) \propto v^2/c^2$ in photon time transfer ($t_{jk}^{(0)} = L_{jk}/c$) after a year. We recall that, in paper (Chauvineau et al. 2005) where the time transfer of photons between LISA spacecraft was studied for a classical LISA orbit, the zeroth order amounted to about 16.7 s ($5 \cdot 10^6$ km/c, that is the nominal interferometric arm-length, L , traveled at the speed of light) with a flexing amplitude of about 0.16 s (48000 km/c); the half order amounted to about $3 \cdot 10^{-3}$ s (960 km/c); and the first order was less than about $1 \cdot 10^{-7}$ s (≤ 30 m/c). Hence, we understand the relevance of relativistic orbit model in

the TDI approach, for a coherent modelling of the mission over a few months.

4. An analytical *development* in eccentricity to check the numerical relativistic versus classical orbit model

Let us find an analytical check of the (relativistic - classical) numerical integration in the eccentric spherical symmetric case, up to first order in e and GM/c^2 . At the post-Newtonian level the solution is known in terms of osculating elements or other representations (e.g. in (Brumberg 1991) or Annex 2 in (Soffel 1989)), valid for any eccentricity. However, those are implicit solutions (for the radial distance and polar angle) and a further development in eccentricity would be relevant to the LISA mission. Indeed, in present LISA literature, orbits and Time Delay Interferometry (TDI) are considered at different levels of approximation, based on a (classical) development in terms of the small eccentricity of the LISA mission (an orbit development at a first-order in eccentricity is further assumed by (Arnaud et al. 2007)). For example, to be ideally a 100 percent efficient in removing laser frequency noise and optical bench noises, the TDI combinations from 1st generation TDI algebra assume symmetric and constant (in time) photon propagation time between two LISA spacecraft. This is met only by a rigid motionless constellation model. Hence the need for a 1.5th TDI generation algebra, this time relaxing the symmetry on time-delays. The latter TDI assumptions being met by modeling the constellation as rotating around its center of mass, and around the Sun (without any planet present) in a Keplerian motion at first order in eccentricity. Deviations from this 1st order in eccentricity Keplerian model lead to residual laser frequency and optical bench noise in the TDI combinations, which need to be quantified. Consequently, the *explicit* general relativistic solution provided in this section as a development at 1PN and first order in eccentricity is useful for the sake of comparison with existing LISA classical models. Our analytical development provides the explicit ($\delta r_k \equiv r_{k\ rel} - r_{k\ cl}$, $\delta \theta_k \equiv \theta_{k\ rel} - \theta_{k\ cl}$) relativistic upgrade to the Keplerian 1st order in eccentricity orbit model for LISA such as used by the LMDC (Arnaud et al. 2007).

To proceed, we first develop the geodesic equation of motion (5) up to the corresponding order in GM/c^2 in the BCRS. Writing $\varepsilon^l \equiv x_{rel}^l - x_{cl}^l$, we find

$$\begin{aligned}
\frac{d^2 x_{rel}^l(t)}{d(ct)^2} &\simeq -\Gamma_{00}^l(x_{rel}^m(t)) + \Gamma_{00}^0(x_{rel}^m(t)) \cdot \frac{v_{rel}^l(t)}{c} \\
&\quad + 2 \left[\begin{array}{l} +\Gamma_{0p}^0(x_{rel}^m(t)) \cdot \frac{v_{rel}^l(t)}{c} \\ -\Gamma_{0p}^l(x_{rel}^m(t)) \\ -\frac{1}{2} \cdot \Gamma_{qp}^l(x_{rel}^m(t)) \cdot \frac{v_{rel}^q(t)}{c} \end{array} \right] \cdot \frac{v_{rel}^p(t)}{c} \\
&\simeq -\Gamma_{00}^l(x_{cl}^m(t)) - \varepsilon^p(t) \cdot \frac{\partial \Gamma_{00}^l(x_{cl}^m(t))}{\partial x_{cl}^p} + \Gamma_{00}^0(x_{cl}^m(t)) \cdot \frac{v_{cl}^l(t)}{c} \\
&\quad + 2 \left[\begin{array}{l} +\Gamma_{0p}^0(x_{cl}^m(t)) \cdot \frac{v_{cl}^l(t)}{c} \\ -\Gamma_{0p}^l(x_{cl}^m(t)) \\ -\frac{1}{2} \cdot \Gamma_{qp}^l(x_{cl}^m(t)) \cdot \frac{v_{cl}^q(t)}{c} \end{array} \right] \cdot \frac{v_{cl}^p(t)}{c}
\end{aligned}$$

where $v^l \equiv dx^l/dt$ is the velocity of spacecraft at time t in the BCRS. Using the analytical developments of Christoffel symbols in the BCRS at the corresponding order, we can write the difference between the relativistic and classical orbit accelerations $d^2\varepsilon^l/dt^2$ as

$$\begin{aligned}
\frac{d^2\varepsilon^l}{dt^2} + \frac{(1)^{lm}}{A} \cdot \varepsilon^m &= \frac{(2)^l}{A} \\
&\text{with} \\
\frac{(1)^{lm}}{A} &= \frac{GM}{r_{cl}^3} \cdot \left[\delta^{lm} - \frac{3x_{cl}^l x_{cl}^m}{r_{cl}^2} \right] \\
\frac{(2)^l}{A} &= \frac{GM}{r_{cl}^3} \cdot \left[\left(\frac{4GM}{r_{cl} c^2} - \frac{v_{cl}^2}{c^2} \right) x_{cl}^l + 4 \frac{v_{cl}^l}{c} \frac{v_{cl}^m}{c} x_{cl}^m \right] \quad (6)
\end{aligned}$$

where r is the coordinate radial distance relative to the Sun at time t in the BCRS and (s) means that the term considered is of order s in GM/c^2 .

Since we consider a symmetric gravitational field and are interested in the difference between relativistic and classical ephemerides for a given satellite, the inclination i is irrelevant. Hence, we choose to work with $i = 0$. The inclined analytical solution can be obtained by a simple rotation of the uninclined analytical solution (11, 12). Then of course, $z_{cl} = z_{rel} = \varepsilon^3 = 0$, as well as the corresponding time derivatives.

Let us further use the set of polar coordinates (r, θ) with $x = r \cos \theta$, $y = r \sin \theta$ and $z = 0$ to reflect the symmetry of the problem. The above set of equations (6) becomes

$$\begin{aligned}
r_{cl} \cdot \delta \ddot{\theta} + 2 \dot{r}_{cl} \cdot \delta \dot{\theta} + 2 \dot{\theta}_{cl} \cdot \delta \dot{r} + \ddot{\theta}_{cl} \cdot \delta r &= \frac{4GM}{c^2} \frac{\dot{r}_{cl}}{r_{cl}} \dot{\theta}_{cl} \quad (7) \\
\delta \ddot{r} - \left[\ddot{\theta}_{cl}^2 + \frac{2GM}{r_{cl}^3} \right] \cdot \delta r - 2 r_{cl} \dot{\theta}_{cl} \cdot \delta \dot{\theta} &= \frac{4GM}{c^2} \cdot \left[\frac{GM}{r_{cl}^3} - \frac{v_{cl}^2}{4 r_{cl}^2} + \frac{\dot{r}_{cl}^2}{r_{cl}^2} \right]
\end{aligned}$$

(8)

where $\delta\theta \equiv \theta_{rel} - \theta_{cl}$, $\delta r \equiv r_{rel} - r_{cl}$ and $\dot{*} \equiv d*/dt$.

Using Kepler's orbital motion equations ($r_{cl} = a(1 - e^2)/(1 + e \cos \theta_{cl})$, $r_{cl}^2 \dot{\theta} = \sqrt{GM a (1 - e^2)}$, $v_{cl} = \sqrt{GM (2/r_{cl} - 1/a)}$), we can check that equations (7) and (8) lead to two first integrals of the motion:

$$r_{cl}^2 \cdot \delta \dot{\theta} + 2 r_{cl} \cdot \dot{\theta}_{cl} \cdot \delta r + \frac{4GM}{r_{cl} c^2} \sqrt{GM a (1 - e^2)} = C_k \quad (9)$$

$$\dot{r}_{cl} \cdot \delta \dot{r} + \left[r_{cl} \cdot \dot{\theta}_{cl}^2 + \frac{GM}{r_{cl}^2} \right] \cdot \delta r + r_{cl}^2 \dot{\theta}_{cl} \cdot \delta \dot{\theta} + \frac{GM}{c^2} \left[-\frac{GM}{r_{cl}^2} + 3 \frac{v_{cl}^2}{r_{cl}} \right] = D_k \quad (10)$$

Those can be traced back to the relativistic angular momentum and energy integral resulting from the spherical symmetry.

Owing to our choice of identical positions and velocities of spacecraft at initial time for both the classical and the relativistic orbit models, $(\delta\theta, \delta r, \delta \dot{\theta}, \delta \dot{r})_{t_0} = (0, 0, 0, 0)$. Hence the integration constants are

$$C_k = 4 \frac{GM}{c^2} \frac{\sqrt{GM a (1 - e^2)}}{r_{k \ cl \ 0}}$$

$$D_k = \frac{GM}{c^2} \left[3 \frac{v_{k \ cl \ 0}^2}{r_{k \ cl \ 0}} - \frac{GM}{r_{k \ cl \ 0}^2} \right]$$

with $r_{k \ cl \ 0} \equiv r_{k \ cl}(t_0)$ and $v_{k \ cl \ 0} \equiv v_{k \ cl}(t_0)$ given by Kepler's orbital equation of motion at initial time with respect to the initial conditions of a given spacecraft $k = 1, 2$ or 3 . Equations (9, 10) provide a first check of the numerical results of Sections 3.4.1 and 3.4.2 in the spherical symmetric approximation. We note that for a circular orbit of reference ($n_{cl} = \dot{\theta}_{cl}$, $r_{cl} = a$, $\dot{r}_{cl} = 0$), C_k and the third term of the left-hand-side of (9) cancel; while D_k and the fourth term of the left-hand-side of (10) cancel... leading to the same identical first integral: $\delta \dot{l} = -2 n_{cl} \delta r$, where $\delta l \equiv r_{rel} \cdot \delta \theta$.

We now develop the differential system ((7) and (8); or, which is easier, (9) and (10)), up to first order in e using Kepler's equations of motion at first order in e :

$$\frac{C_k}{a n_{cl}} = (1 - 2 e \cos \theta_{cl}) \cdot \delta \dot{l} + 2 (1 + e \cos \theta_{cl}) \cdot \delta r + \frac{4GM}{c^2} (1 + e \cos \theta_{cl})$$

$$\frac{D_k}{a n_{cl}^2} = \delta \dot{l} + e \sin \theta_{cl} \cdot \delta \dot{r} + (2 + 5 e \cos \theta_{cl}) \cdot \delta r + \frac{GM}{c^2} (2 + 7 e \cos \theta_{cl})$$

with $' \equiv d*/d(n_{cl}t)$. To find solutions to the above differential system, we use the theory of perturbation around null eccentricity. We find

$$\begin{aligned} \delta\theta_k &\simeq \delta\theta_k^{[0]} + \delta\theta_k^{[1]} \\ &\text{with} \\ \delta\theta_k^{[0]} &= -6 \frac{GM}{a c^2} \left\{ \begin{array}{l} +n_{cl}t - \cos(n_{cl}t_{kp}) \sin(n_{cl}(t - t_{kp})) \\ -\sin(n_{cl}t_{kp}) \cos(n_{cl}(t - t_{kp})) \end{array} \right\} \\ \delta\theta_k^{[1]} &= +e \frac{GM}{a c^2} \left\{ \begin{array}{l} +2 \sin(n_{cl}t_{kp}) - 21 \cos(n_{cl}t_{kp}) n_{cl}t \\ -18 n_{cl}t \cos(n_{cl}(t - t_{kp})) \\ +22 \cos(n_{cl}t_{kp}) \sin(n_{cl}t_{kp}) \cos(n_{cl}(t - t_{kp})) \\ + \{2 + 22 \cos^2(n_{cl}t_{kp})\} \sin(n_{cl}(t - t_{kp})) \\ +15 \sin(n_{cl}t_{kp}) \cos^2(n_{cl}(t - t_{kp})) \\ +15 \cos(n_{cl}t_{kp}) \sin(n_{cl}(t - t_{kp})) \cos(n_{cl}(t - t_{kp})) \end{array} \right\} \end{aligned} \quad (11)$$

$$\begin{aligned} \delta r_k &\simeq \delta r_k^{[0]} + \delta r_k^{[1]} \\ &\text{with} \\ \delta r_k^{[0]} &= +3 \frac{GM}{c^2} \left\{ \begin{array}{l} +1 - \cos(n_{cl}t_{kp}) \cos(n_{cl}(t - t_{kp})) \\ +\sin(n_{cl}t_{kp}) \sin(n_{cl}(t - t_{kp})) \end{array} \right\} \\ \delta r_k^{[1]} &= +e \frac{GM}{c^2} \left\{ \begin{array}{l} +20 \cos(n_{cl}t_{kp}) - 9 n_{cl}t \sin(n_{cl}(t - t_{kp})) \\ - \{3 + 11 \cos^2(n_{cl}t_{kp})\} \cos(n_{cl}(t - t_{kp})) \\ +11 \cos(n_{cl}t_{kp}) \sin(n_{cl}t_{kp}) \sin(n_{cl}(t - t_{kp})) \\ -6 \cos(n_{cl}t_{kp}) \cos^2(n_{cl}(t - t_{kp})) \\ +6 \sin(n_{cl}t_{kp}) \sin(n_{cl}(t - t_{kp})) \cos(n_{cl}(t - t_{kp})) \end{array} \right\} \end{aligned} \quad (12)$$

where $[s]$ means that the term considered is of order s in e . At zeroth order in e , those results correspond to the circular classical orbit of reference case.

Expressions (11) and (12) can be easily transposed in terms of (relativistic - classical) positions $(\delta x_k, \delta y_k)$ and related (relativistic - classical) coordinate velocities $(\delta \dot{x}_k, \delta \dot{y}_k)$ using

$$\begin{cases} x_k = r_k \cos \theta_k \\ y_k = r_k \sin \theta_k \end{cases} \Rightarrow \begin{cases} \delta x_k = \cos \theta_k \cdot \delta r_k - r_k \sin \theta_k \cdot \delta \theta_k \\ \delta y_k = \sin \theta_k \cdot \delta r_k + r_k \cos \theta_k \cdot \delta \theta_k \end{cases} .$$

4.1. CIRCULAR CLASSICAL REFERENCE ORBIT CASE:

Expressions (11) and (12) with $e = 0$ match perfectly the numerical results for the circular spherical symmetric case presented in Section 3.4.1, up to first order in GM/c^2 . Residuals between RMI approach and this analytical check for the circular spherical symmetric case reach about 1 cm in x-y-positions or along track distance and a few millimeters in radius (Figures 9 and 10).

A dimensional analysis leads to an order of magnitude for the difference between classical and relativistic barycentric positions of spacecraft of about $GM/(ac^2) \cdot 2\pi a \simeq 10$ km for a one year simulation. Our numerical native relativistic approach shows that classical modelling can be wrong by as much as about 50 km, in terms of barycentric coordinates (x,y,z) and along track distance, over one year. It is interesting to point out that this is nearly one order of magnitude larger than estimated with a dimensional analysis. The numerical results are confirmed by the more cautious analytical developpements presented above.

4.2. ECCENTRIC CLASSICAL REFERENCE ORBIT CASE

Expressions (11) and (12) with orbital elements corresponding to LISA's ($e = 0.0096$) but $i = 0$ match the numerical results for the eccentric spherical symmetric case presented in Section 3.4.2, up to first order in e and in GM/c^2 .

Residuals between the RMI approach and this analytical check *at zeroth order in e* , for the eccentric spherical symmetric case, reach up to about +840, ± 540 or -800 m in radial distance and about -3600 , $+2400$ or $+1600$ m in along track distance, for spacecraft $k = 1, 2$ or 3 respectively, over a year (Figures 11 and 12).

When the analytical check for the eccentric spherical symmetric case is considered *up to first order in e* , the residuals reach up to about $+24$, -15 or $+14$ m in radius and about -85 , -25 or $+32$ m in along track distance, for spacecraft $k = 1, 2$ or 3 respectively, over a year (Figures 13 and 14). Residuals between the RMI numerical analysis (implicitly containing all orders in e) and the analytical development (up to first order in e , equations (11) and (12)) are bound to be larger for space missions with larger eccentricities than that of LISA's ($e_{LISA} \simeq 0.0096$). This shows the limits of the analytical development even for an *eccentric* model with a simple spherical symmetric gravitational field. And going to higher orders in e increases the number of terms in expressions (11) and (12) drastically, as illustrated by the 0-th and 1-st order contributions. Non symmetric cases such as in presence of planets, with a central body which is non spherical or has a spin, are even much more complex to handle analytically. On the opposite, the

RMI approach, which is exact in terms of e , implicit in terms of spin, flattening or planets, via the metric, is very flexible. Indeed, RMI also runs when the spherical symmetry is broken, since solar spin, multipolar development of the solar mass, point-like planets can be introduced in the metric and hence be coherently taken into account in numerical ephemerides produced for LISA via that approach.

5. Conclusions

The aim of the present paper was to illustrate how the Relativistic Motion Integrator (RMI) can be used to provide a relativistic numerical satellite (or test-body) propagator for space missions; and to quantify relativistic effects when a comparison is made with a classical corresponding model.

As an illustration of RMI and to validate the method, we chose the space interferometer LISA, modelled in the Barycentric Coordinate Reference System (BCRS) in the gravitational field of a spherical non-rotating Sun, without planets (the spherical symmetric case). We compared the numerical relativistic ephemeris (propagated daily positions and velocities of each spacecraft) obtained with RMI to the ones obtained with a classical numerical model with identical initial conditions in terms of positions and velocities. The (relativistic - classical) BCRS position obtained seemed a priori large, up to a few tenth kilometers, i.e. more or less 5 or 6 times the estimate obtained from a rapid dimensional analysis.

However, we made a careful analytical analysis: analytical expressions (up to first order in GM/c^2 , with G , Newton's constant, M , the Sun's mass and c , the speed of light in vacuum) of two first integrals of the problem and an analytical development of (relativistic - classical) BCRS along track and radial distances up to first order in eccentricity e and in GM/c^2 . The analytical developments with orbital elements corresponding to LISA's confirmed the numerical results obtained and validates the RMI approach. The difference between the RMI numerical approach, based on the exact relativistic equation of motion with respect to the BCRS metric (which is up to second order in GM/c^2 in the IAU2000 resolutions) for a spherical non-rotating Sun, and the analytical development are of order $e^2 \cdot GM/c^2$.

Hence, for LISA, we have shown that, when the classical orbit of reference is eccentric with $e_{LISA} \simeq 0.0096$, the difference between relativistically and classically modelled radial distance reaches up to a maximum of about 8 – 9 km during a one-year mission. After one year (i.e. one classical period), the difference in orbits in terms of radial distance can

be as much as about 680 m and along track difference is about 54 – 59 km according to the spacecraft considered.

Errors in LISA satellite orbit may have consequences when modelling LISA’s arm flexing for the sake of interferometry. We showed that a relativistic orbit model is relevant when studying photon time transfer needed in the TDI method. Using a classical orbit model contributes to an error of about 10^{-5} s (≈ 3 km/ c) in photon time transfer over a year. The TDI method is the crucial pre-processing of LISA data, before even trying a given strategy to detect any gravitational wave signal.

Since the orders of magnitude of $(a_k, e_k, i_k)_{k=1,2,3}$ used in Hughes orbit model for LISA’s three spacecraft (Hughes 2005) are the same as the ones chosen here, the same conclusions will apply in Hughes’ case.

Note that, in the present paper, we did not aim at a complete model of the LISA detector, but some of the above result might be interesting when building a LISA simulator.

Our present study also shows that while the analytical development soon reaches its limits, the strength of the RMI approach is that it also runs when the spherical symmetry is broken ($i \neq 0$, non-spherical Sun, rotating Sun, with planets), cases much more complex to model analytically. Indeed, a solar spin or multipolar development of the solar mass (solar J_2) or point-like planets can be introduced in the metric and hence be coherently taken into account in numerical ephemerides produced for LISA via the RMI approach. The point is to use a metric with a sufficiently high order of development in $1/c^2$, so as to include all the classical and relativistic effects relevant to the precision of the space mission considered. The IAU 2000 BCRS metric models coherently, for LISA and other space missions, the action of the Sun and planets at a relativistic level.

Finally, the RMI approach can be applied to other space missions, whether barycentric or planetocentric.

6. FIGURES

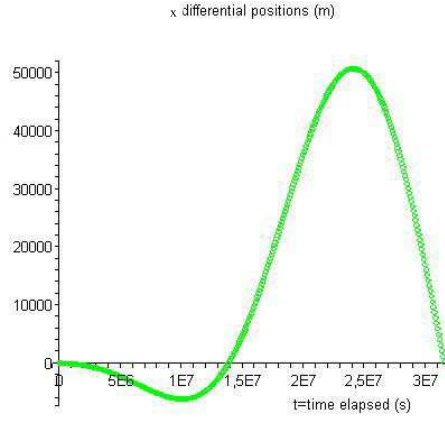


Figure 1. Difference between numerical relativistic and classical position ephemerides for the LISA mission in the *circular* spherical symmetric case: x barycentric coordinate (δx).

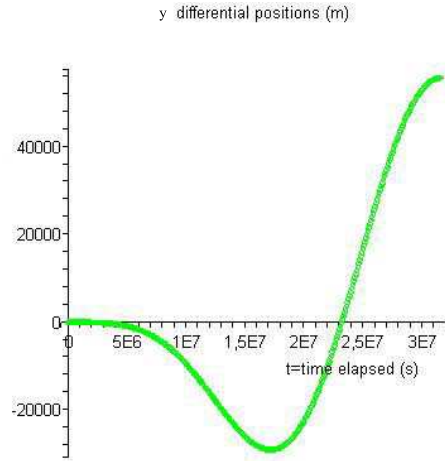


Figure 2. Difference between numerical relativistic and classical position ephemerides for the LISA mission in the *circular* spherical symmetric case: y barycentric coordinate (δy).

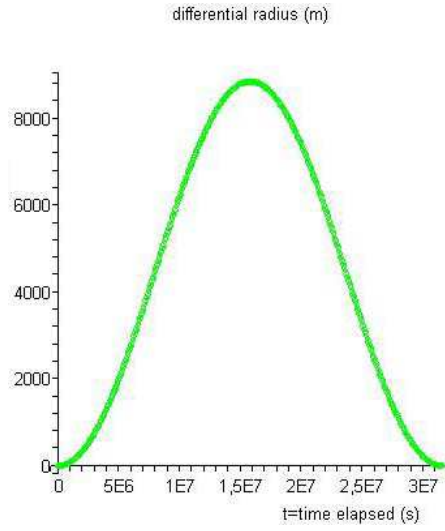


Figure 3. Difference between numerical relativistic and classical position ephemerides for the LISA mission in the *circular* spherical symmetric case: radial barycentric distance (δr).

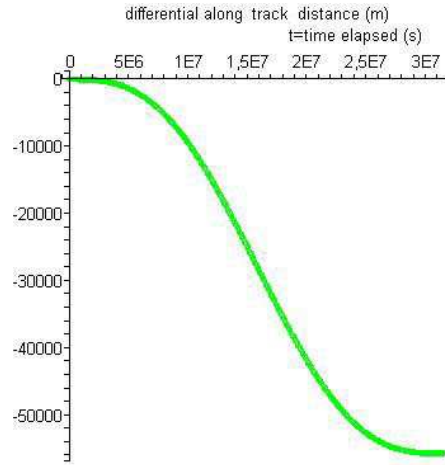


Figure 4. Difference between numerical relativistic and classical position ephemerides for the LISA mission in the *circular* spherical symmetric case: along track distance ($\delta l \equiv r_{rel} \cdot \delta \theta \simeq a \cdot \delta \theta$).

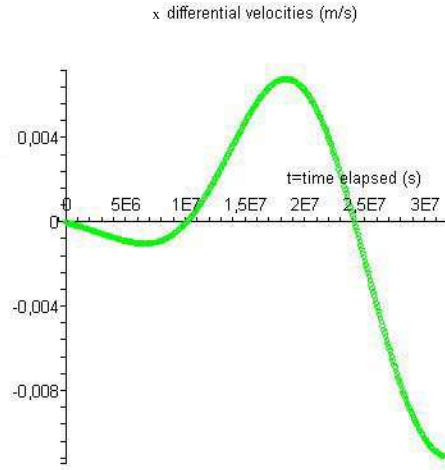


Figure 5. Difference between numerical relativistic and classical velocity ephemerides for the LISA mission in the *circular* spherical symmetric case: velocity component along the x barycentric coordinate axis ($\delta \dot{x}$).

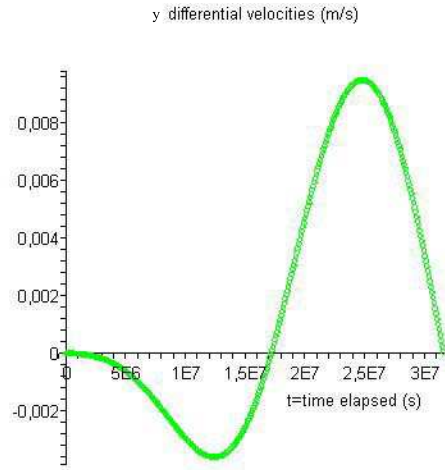


Figure 6. Difference between numerical relativistic and classical velocity ephemerides for the LISA mission in the *circular* spherical symmetric case: velocity component along the y barycentric coordinate axis ($\delta \dot{y}$).

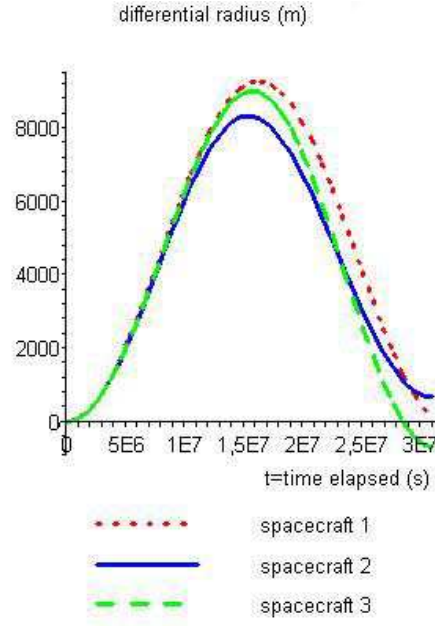


Figure 7. Difference between numerical relativistic and classical position ephemerides for the LISA mission in the *eccentric* ($e_{LISA} \simeq 0.0096$) spherical symmetric case: radial barycentric distance (δr).

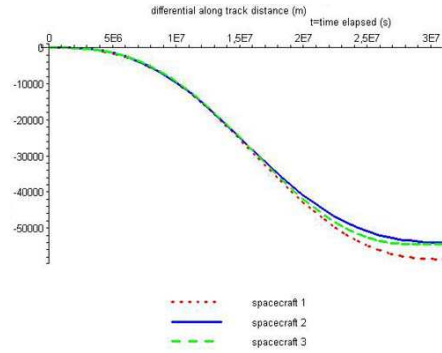


Figure 8. Difference between numerical relativistic and classical position ephemerides for the LISA mission in the *eccentric* ($e_{LISA} \simeq 0.0096$) spherical symmetric case: along track distance (δl).

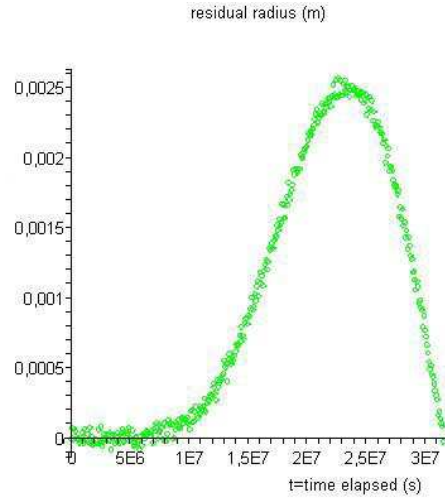


Figure 9. Residuals between the numerical (relativistic - classical) position ephemerides and the corresponding analytical development for the LISA mission in the *circular* ($e = 0$) spherical symmetric case: radial distance (δr).

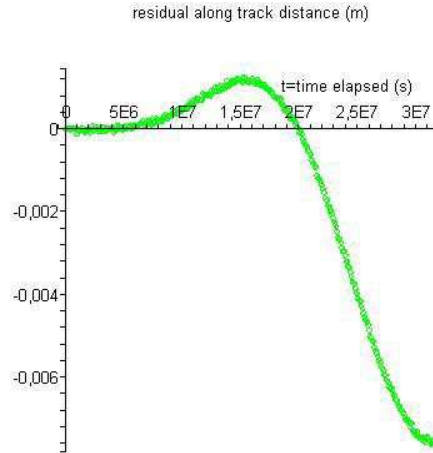


Figure 10. Residuals between the numerical (relativistic - classical) position ephemerides and the corresponding analytical development for the LISA mission in the *circular* ($e = 0$) spherical symmetric case: along track distance (δl).

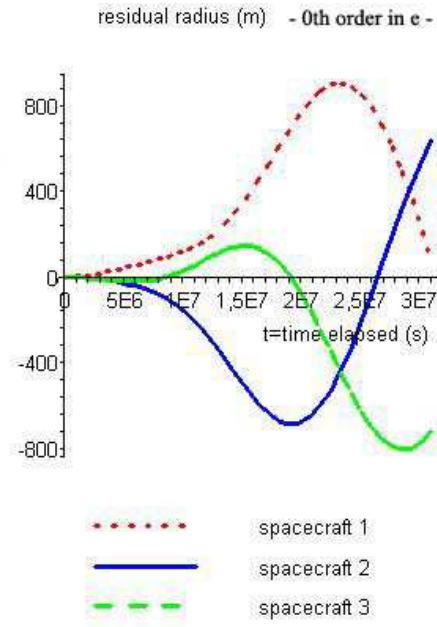


Figure 11. Residuals between the numerical (relativistic - classical) position ephemerides and the corresponding analytical development at 0th order in e for the LISA mission in the *eccentric* ($e_{LISA} \simeq 0.0096$) spherical symmetric case: radial distance (δr).

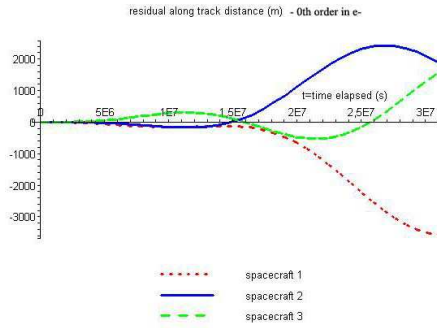


Figure 12. Residuals between the numerical (relativistic - classical) position ephemerides and the corresponding analytical development at 0th order in e for the LISA mission in the *eccentric* ($e_{LISA} \simeq 0.0096$) spherical symmetric case: along track distance (δl).

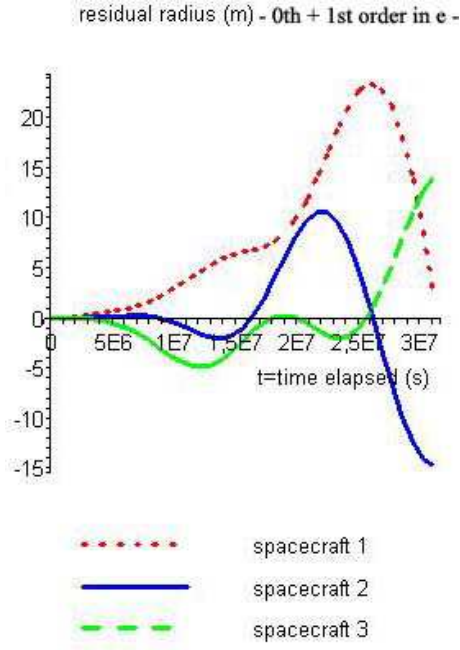


Figure 13. Residuals between the numerical (relativistic - classical) position ephemerides and the corresponding analytical development up to 1st order in e for the LISA mission in the *eccentric* ($e_{LISA} \simeq 0.0096$) spherical symmetric case: radial distance (δr).

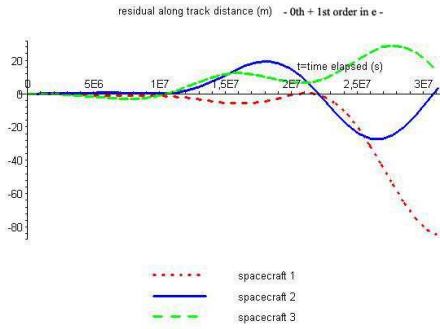


Figure 14. Residuals between the numerical (relativistic - classical) position ephemerides and the corresponding analytical development up to 1st order in e for the LISA mission in the *eccentric* ($e_{LISA} \simeq 0.0096$) spherical symmetric case: along track distance (δl).

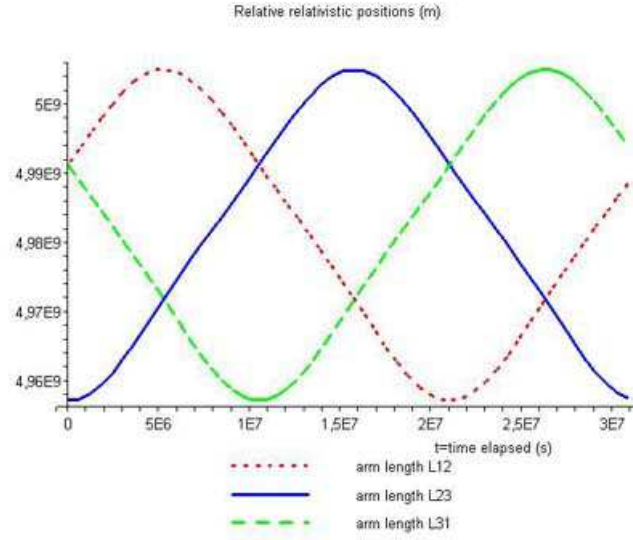


Figure 15. Numerical relativistic modelling of LISA breathing in the *eccentric* spherical symmetric case ($e_{LISA} \simeq 0.0096$): relative positions between spacecraft, with L_{jk} the interdistance between spacecraft $j, k = 1, 2, 3$ where $j \neq k$.

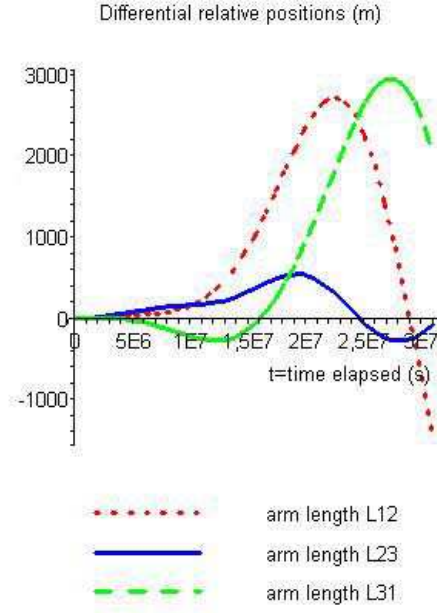


Figure 16. Difference between numerical relativistic and classical modelling of LISA breathing in the *eccentric* spherical symmetric case ($e_{LISA} \simeq 0.0096$): difference in relative positions between spacecraft, with L_{jk} the interdistance between spacecraft $j, k = 1, 2, 3$ where $j \neq k$.

Appendix

A. Numerical estimate of the Christoffel Symbols

Within a numerical integration of the relativistic equations of motion, one has to carefully check the numerical accuracy. In this section, we show that the numerical errors are smaller than the order of magnitude of the relativistic effects.

In order to integrate equation (3), we need to evaluate numerically the Christoffel Symbols

$$\Gamma_{\mu\nu}^{\alpha} = \frac{1}{2} g^{\alpha\beta} (g_{\beta\nu,\mu} + g_{\mu\beta,\nu} - g_{\mu\nu,\beta}) \quad (13)$$

where $f_{,x} = \frac{\partial f}{\partial x}$ and the matrix $g^{\alpha\beta}$ is the inverse of the matrix $g_{\alpha\beta}$ owing to expression (4). We need to evaluate numerically the derivative, $g_{\mu\nu,\beta}$, of the metric components. The derivative is computed using an estimation of order 4 (Kincaid & Cheney 2002)

$$D_h(x) = \frac{f(x-2h) - 8f(x-h) + 8f(x+h) - f(x+2h)}{12h} \quad (14)$$

$$\text{with } f'(x) = D_h(x) + \mathcal{O}(h^4) \quad (15)$$

As can be seen in Figure 17, one needs to choose the discretisation step size, h , very carefully. For large h , the discretisation error is important ($\propto h^4$) but for small h , the roundoff error increases ($\propto 1/h$).

In order to increase the precision of the derivative, it is usefull to derive $h_{\mu\nu} = g_{\mu\nu} - \eta_{\mu\nu}$, where $\eta_{\mu\nu}$ is the Minkowsky metric, instead of $g_{\mu\nu}$ as it is more stable from a numerical point of view (Figure 17).

It is also interesting to use Richardson extrapolation (Richardson & Gaunt 1927). This requires two estimations of order 4 ($D_{0,0} = D_h(x)$ and $D_{1,0} = D_{h/k}(x)$ where k is a real factor) to construct a new estimation of order 8:

$$D_{1,1} = \frac{k^4 D_{1,0} - D_{0,0}}{k^4 - 1} \quad (16)$$

In practice, the factor k is choosen as 1.5 or 2 and this procedure can be iterated starting from $D_{i,0} = D_{h/k^i}$ to construct the new estimation

$$D_{i,j} = \frac{k^{4j} D_{i,j-1} - D_{i-1,j-1}}{k^{4j} - 1} \quad (17)$$

After n steps, $D_{n,n}$ is of the order of $\mathcal{O}(h^{4(n+1)})$. Figure 17 illustrates in the case of LISA how a relative error of order of 10^{-14} on the

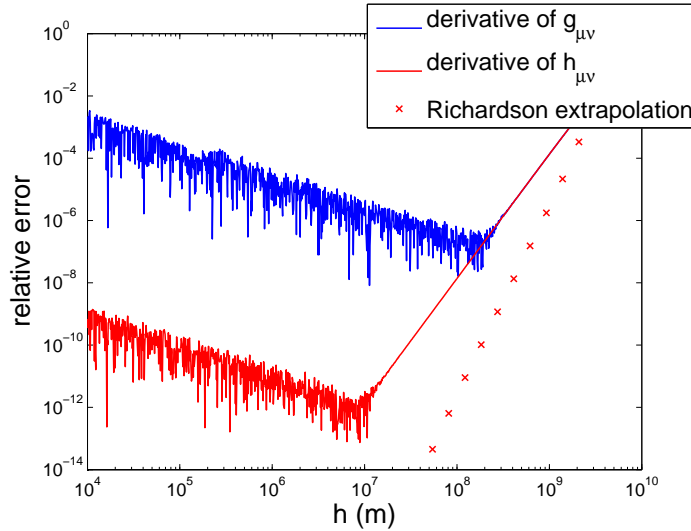


Figure 17. Representation of the relative precision of $g_{tt,x}$ for one point of the LISA orbit. The relative precision of $g_{tt,x}$ and $h_{tt,x}$ are represented as function of the discretisation step, h . The Richardson extrapolation is also represented for a factor $k = 1.5$ (12 iterations are represented).

derivative of $h_{\mu\nu}$ can be reached (in double precision) using Richardson extrapolation. This method does not require to start with a very fine tuned initial step size h and it is possible to stop the iterations when the convergence is sufficient.

B. Acknowledgments

S. Pireaux acknowledges a CNES (Centre National d'Etudes Spatiales, France) post-doctoral grant, plus a one-month contract at the Observatoire de la Côte d'Azur (OCA, France) as financial support for most part of her work relevant to the present paper. A. Hees is research fellow from FRS-FNRS (Belgian Fund for Scientific Research) for his thesis at ORB-UCL (Observatoire Royal de Belgique - Université Catholique de Louvain, Belgium).

References

- Arnaud, K. A., Babak, S., Baker, J. G., Benacquista, M. J., Cornish, N. J., Cutler, C., Finn, L. S., Larson, S. L., Linttberg, T., Porter, E. K., Vallisneri, V., Vecchio, A., Vinet, J-Y. (the Mock LISA Challenge Task Force): An overview of the second round of the LISA Mock Data Challenges, arXiv:0701170v4(gr-qc) (2007)

- Brumberg, V.: Essential relativistic celestial mechanics. Hilger, Bristol (1991).
- Brumberg, V.: Relativistic geocentric satellite equations of motion in closed form. *Astronomy and Astrophysics*, 257, 2, 777-782 (1992).
- Brumberg, V.: On Relativistic Equations of Motion of an Earth Satellite. *Celestial Mechanics and Dynamical Astronomy*, 88, 2, 209-225 (2004)
- Brumberg, V.: On derivation of EIH (EinsteinInfeldHoffman) equations of motion from the linearized metric of general relativity theory, *Celestial Mechanics and Dynamical Astronomy*, 99, 3, 245-252 (2007)
- Chauvineau, B., Regimbau, T., Vinet, J-Y., Pireaux, S.: Relativistic analysis of the LISA long range optical links. *Phys. Rev. D*, 72, 122003 (2005); gr-qc/0511157
- Ciufolini, I., Pavlis, E. C.: A confirmation of the general relativistic prediction of the Lense-Thirring effect. *Nature*, 431, 7011, 958-960 (2004)
- Cornish, N. J., Rubbo, L. J., Poujade, O.: Forward modeling of space-borne gravitational wave detectors, *Phys. Rev. D*, 69, 082003 (2004)
- Damour, T., Soffel, M. and Xu, C.: General-relativistic celestial mechanics. I. Method and definition of reference systems. *Phys. Rev. D*, 43, 3273-3307 (1991)
- Damour, T., Soffel, M. and Xu, C.: General-relativistic celestial mechanics II. Translational equations of motion. *Phys. Rev. D*, 45, 1017-1044 (1992)
- Damour, T., Soffel, M. and Xu, C.: General-relativistic celestial mechanics. III. Rotational equations of motion. *Phys. Rev. D*, 47, 3124-3135 (1993)
- Damour, T., Soffel, M. and Xu, C.: General-relativistic celestial mechanics. IV. Theory of satellite motion. *Phys. Rev. D*, 49, 618-635 (1994)
- Dhurandhar, S.V., Nayak, K.R., Vinet, J-Y.: Algebraic approach to time-delay data analysis for LISA. *Phys. Rev. D* 65, 102002 (2002)
- Dhurandhar, S., Nayak, K.R., Vinet, J-Y.: Fundamentals of the LISA stable flight formation. *CQG*, 22, 481-487 (2005)
- Estabrook, F.B., Tinto, M., Armstrong, J.W.: Time-delay analysis of LISA gravitational wave data: Elimination of spacecraft motion effects. *Phys. Rev. D*, 62, 042002 (2000)
- Hees, A., Pireaux, S.: A Relativistic Motion Integrator: Numerical accuracy and illustration with BepiColombo and MarsNext, *Proceedings of the IAU Symposium* 261, 26th April-1st May, Virginia, USA (2009)
- Hughes, S. P.: Preliminary optimal orbit design for the Laser Interferometer Space Antenna LISA. AAS 02-2005, Flight Dynamics Analysis Branch, NASA Goddard Space Flight Center (2005)
- Kincaid, D., and Cheney, W., *Numerical analysis: Mathematics of Scientific Computing*, American Mathematical Society (2002)
- Klioner, S.: Relativistic perturbations for Lissajous orbits around L2. *GAIA Gaia Technical Report* (2005). Available from the Gaia document archive <http://www.rssd.esa.int/link/livelink>
- LISA: a cornerstone mission for the observation of gravitational waves. *System and Technology Study Report* (2000)
- LISA-France web site at <http://www.apc.univ-paris7.fr/LISA-France/analyse.phtml>
- Moyer, T. D.: Formulation for observed and computed values of Deep Space Network data types for Navigation. *Monograph 2, Deep Space Communications and Navigation Series*, JPL, USA (2000)
- Nayak, K.R., Koshti, S., Dhurandhar, S.V., Vinet, J-Y.: On the minimum of LISA's arm flexing. *CQG*, 23, 1763-1778 (2006); Reducing the flexing of the arms of LISA, gr-qc/0507105 v1

- Petiteau, A., Auger, G., Halloin, H., Jeannin, O., Pireaux, S., Plagnol, E., Regimbaut, T., Vinet, J.-Y.: LISACode: A scientific simulator of LISA, *Phys. Rev. D*, 77023002 (2008)
- Pireaux, S., Barriot, J.-P., Rosenblatt, P., Benna, M.: Integrating the motion of satellites in a consistent relativistic framework. The SCRMI prototype software. Flight Mechanics Symposium, 18-20th October 2005, Goddard Space Flight Center, USA, NASA conference publication NASA/CP-2005-212789
- Pireaux, S., Barriot, J.-P., Rosenblatt, P.: SCRMI: a Semi-Classical Relativistic Motion Integrator, to model the orbits of space probes around the Earth and other planets. *Acta Astronautica*, 59, 517-523 (2006); gr-qc/06022008
- Pireaux, S.: Time scales in LISA. *CQG*, 24, 2271-2281 (2007)
- Richardson, L. F. and Gaunt, J. A., The Deferred Approach to the Limit. Part I. Single Lattice. Part II. Interpenetrating Lattices, *Royal Society of London Philosophical Transactions Series A*, 226, 299-361 (1927), <http://adsabs.harvard.edu/abs/1927RSPTA.226..299R>
- Soffel, M.: *Relativity in Astrometry, Celestial Mechanics and Geodesy*. Springer-Verlag (1989).
- Soffel, M., Klioner, S. A., Petit, G., Wolf, P., Kopeikin, S. M., Bretagon, P., Brumberg, V. A., Capitaine, N., Damour, T., Fukushima, T., Guinot, B., Huang, T., Lindegren, T., Ma, C., Nordtvedt, K., Ries, J., Seidelmann, P. K., Vokrouhlicky, D., Will, C., Xu, C.: The IAU 2000 resolutions for astrometry, celestial mechanics and metrology in the relativistic framework: explanatory supplement. *Astron. J.*, 126, 6, 2687-2706 (2003); astro-ph/0303376v1
- Vallisneri, M.: Synthetic LISA: simulating time delay interferometry in a model LISA, *Phys. Rev. D*, 71, 022001 (2005)